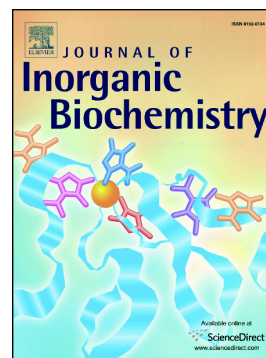


## Accepted Manuscript

The role of ancillary ligand substituents in the biological activity of triruthenium-NO complexes

Camila Fontes Neves da Silva, Bruna Possato, Lilian Pereira Franco, Loyanne Carla Barbosa Ramos, Sofia Nikolaou



PII: S0162-0134(18)30052-7  
DOI: doi:[10.1016/j.jinorgbio.2018.05.021](https://doi.org/10.1016/j.jinorgbio.2018.05.021)  
Reference: JIB 10511

To appear in: *Journal of Inorganic Biochemistry*

Received date: 26 January 2018  
Revised date: 28 May 2018  
Accepted date: 28 May 2018

Please cite this article as: Camila Fontes Neves da Silva, Bruna Possato, Lilian Pereira Franco, Loyanne Carla Barbosa Ramos, Sofia Nikolaou , The role of ancillary ligand substituents in the biological activity of triruthenium-NO complexes. *Jib* (2017), doi:[10.1016/j.jinorgbio.2018.05.021](https://doi.org/10.1016/j.jinorgbio.2018.05.021)

This is a PDF file of an unedited manuscript that has been accepted for publication. As a service to our customers we are providing this early version of the manuscript. The manuscript will undergo copyediting, typesetting, and review of the resulting proof before it is published in its final form. Please note that during the production process errors may be discovered which could affect the content, and all legal disclaimers that apply to the journal pertain.

**The role of ancillary ligand substituents in the biological activity of triruthenium-  
NO complexes**

**Camila Fontes Neves da Silva,<sup>[a]</sup> Bruna Possato,<sup>[a]</sup> Lilian Pereira Franco,<sup>[a]</sup> Lyanne Carla Barbosa  
Ramos,<sup>[b]</sup> and Sofia Nikolaou\*<sup>[a]</sup>**

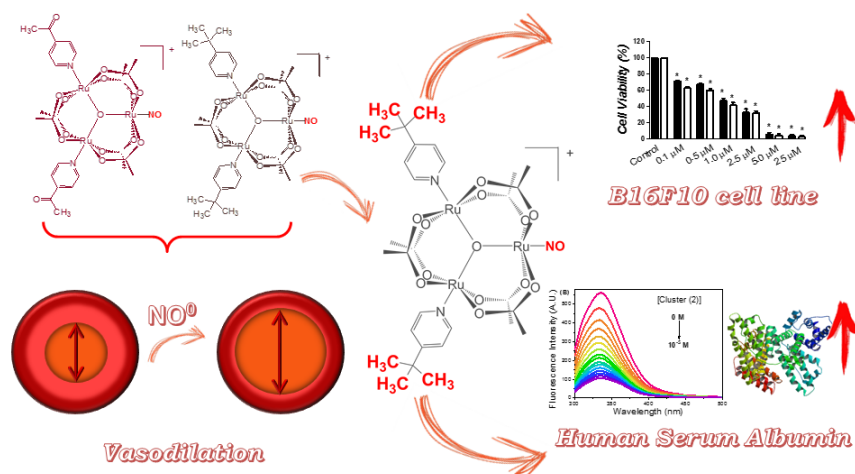
<sup>a</sup>Departamento de Química da Faculdade de Filosofia, Ciências e Letras de Ribeirão Preto – Universidade de São Paulo, Av. Bandeirantes 3900, ZIP-CODE 14040-901, Ribeirão Preto-SP, Brazil, Phone: 55 16 33153748, sofia@ffclrp.usp.br

<sup>b</sup>Faculdade de Ciências Farmacêuticas de Ribeirão Preto - Universidade de São Paulo, Av. Bandeirantes 3900, ZIP-CODE 14040-901, Ribeirão Preto-SP, Brazil.

\*corresponding author: Prof. Sofia Nikolaou, sofia@ffclrp.usp.br.

ACCEPTED MANUSCRIPT

## Graphical Abstract



## Graphical synopsis

$[\text{Ru}_3(\mu_3\text{-O})(\mu\text{-OOCCH}_3)_6(\text{NO})(\text{L})_2]\text{PF}_6$  (L = 4-acetylpyridine, **1** or 4-tert-butylpyridine, **2**) release NO. Vasodilation activity does not depend on ligand L structure; whereas methyl groups on the ancillary ligand of **2** modulate its cytotoxicity to B16F10 murine melanoma cells. Methylation also increases interaction of **2** with HSA (human serum albumin), through hydrophobic forces.

## Highlights

- $[\text{Ru}_3\text{O}(\text{OOCCH}_3)_6(\text{L})_2\text{NO}]^+$  (4-acetylpyridine, **1**; 4-tert-butylpyridine, **2**) were characterized
- Both complexes release NO in solution by photoinduction and/or reductive stimulus
- Both complexes relax pre-contracted rat aorta with maximum efficiency
- Compound **2** is more cytotoxic to B16F10 melanoma cells due its ancillary ligand
- **2** also interacts with human serum albumin more efficiently, through hydrophobic forces

**Abstract**

Two novel triruthenium clusters,  $[\text{Ru}_3(\mu_3\text{-O})(\mu\text{-OOCCH}_3)_6(\text{NO})\text{L}_2]\text{PF}_6$  (L = 4-acetylpyridine, **1**, or 4-tert-butylpyridine, **2**) release NO. Their spectroscopic and electrochemical characterization confirmed their structure. These complexes efficiently deliver NO in solution under irradiation at  $\lambda_{\text{irrad}} = 377$  nm and/or through chemical reduction with ascorbic acid. Clusters **1** and **2** elicit vasodilation and, at concentrations of  $10^{-5}\text{M}$ , can relax up to 100% of pre-contracted rat aorta. Complex **2** is more cytotoxic to murine melanoma B16F10 cells than complex **1**: at 50 times lower concentration than complex **1**, complex **2** decreases cell viability to 50% in the dark or under irradiation with visible light ( $\lambda_{\text{irrad}} = 527$  nm). The higher cytotoxicity of complex **2** can be assigned to its larger hydrophobicity, promoted by the methylated tert-butylpyridine ancillary ligand in its structure. Investigation into Human Serum Albumin (HSA) fluorescence quenching by clusters **1** or **2** revealed that complex **2** quenches HSA luminescence with a very high Stern-Volmer constant ( $K_{\text{SV}} = 9.49 \times 10^7 \text{ M}^{-1}$  at  $T = 298$  K) and suggested that the nature of the interaction between complex **2** and HSA is hydrophobic ( $\Delta H = 80.81 \text{ KJ/mol}$  and  $\Delta S = 334.71 \text{ J/K mol}$ ). HSA lifetime and circular dichroism data pointed to a static quenching mechanism for both complexes. Together, our results show that a hydrophobic substituent in the cluster ancillary ligand improves NO release ability, cytotoxicity, and interaction with a bio-target.

**Keywords:** triruthenium nitrosyl clusters; NO releasing molecules; methylation; vasodilation; anti-cancer activity; HSA fluorescence quenching.

## 1. Introduction

Alfred W. Mond started to study  $\mu$ -oxo trinuclear ruthenium clusters in the 1930s [1]. This subject has been reviewed twice in the past years [2, 3]. These clusters have significant redox and catalytic properties that depend on the substituent present in the ancillary ligands and which are directly related to the ligands pKa [4, 5]. Various applications of these clusters have been reported: they can be used in electronic materials to perform intramolecular electron transfer; they can be employed as precursors for construction of supramolecular assemblies, 3D architectures on electrode surfaces, and nanomaterials; and they have potential biological application as anti-tumor and vasodilation agents [6–17].

Strong electronic mixing based on metal-metal interactions dictates the chemistry of trinuclear ruthenium carboxylates and leads to large electronic delocalization within the  $[\text{Ru}_3\text{O}]^+$  unit [2]. This property allows clusters to react with  $\pi$ -acceptor species like CO and NO due to the intrinsic ability of the latter molecules to perform  $\pi$ -backbonding with the  $[\text{Ru}_3\text{O}]^n$  metal center. This fact has increased interest in applying these compounds as releasing or scavenging agents of relevant biological molecules, including  $\text{CO}_{(g)}$  and  $\text{NO}_{(g)}$ . To date, four literature works have focused on controlled NO release from complexes with general formula  $[\text{Ru}_3(\mu_3\text{-O})(\mu\text{-OOCCH}_3)_6(\text{NO})\text{L}_2]\text{PF}_6$  (where L = pyridinic ligands) [16–20], but other structures and approaches have also been described [21–23].

Both photo and redox stimuli can trigger NO release. Triruthenium complexes undergo up to three redox processes within the potential window that is accessible in physiological medium, so these complexes are potential NO-delivery systems even in the dark. Our group has previously dealt with these aspects without discussing how ancillary ligands influence biological assays [16–18]. To the best of our knowledge, investigating structure-activity relationship is the best way to design new drugs. Medicinal chemistry has already explored the methylation effect [24]. The methyl group ( $-\text{CH}_3$ ) is very important for molecular recognition of organic and inorganic compounds by bioreceptors [25–28]. Furthermore, the  $\text{CH}_3$  group increases the overall lipophilicity of a given molecule and promotes stronger hydrophobic interactions in the case of some compounds [24–28].

This study presents the synthesis and characterization of two novel clusters with general formula  $[\text{Ru}_3(\mu_3\text{-O})(\mu\text{-OOCCH}_3)_6(\text{NO})(\text{L})_2]\text{PF}_6$  (where L = 4-acetylpyridine, 4-acpy (**1**) or 4-tert-butylpyridine, 4-tbpy (**2**), Figure 1) and discusses how the substituent in the ancillary ligand affects the biological activity of clusters **1** and **2**. We have conducted *in vitro* MTT (3-(4,5-dimethylthiazol-2-yl)-2,5-diphenyltetrazolium bromide) assays [29] to evaluate cluster cytotoxicity to two cell lines, L929 (murine fibroblast, a non-tumor cell), and B16F10 (murine melanoma). We have also investigated other biological properties of clusters **1** and **2** including their vasorelaxation capacity and their interaction with HSA (Human Serum Albumin).

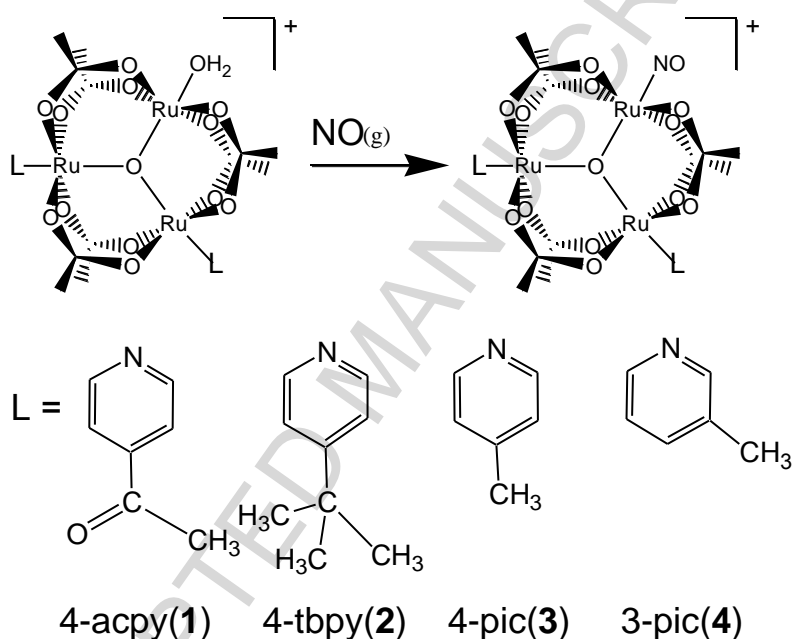


**Figure 1.** Reaction of the precursor  $[\text{Ru}_3(\mu_3\text{-O})(\mu\text{-OOCCH}_3)_6(\text{H}_2\text{O})(\text{L})_2]^+$  with the nitrosyl ligand  $\text{NO}(\text{g})$ , to obtain clusters with the general formula  $[\text{Ru}_3(\mu_3\text{-O})(\mu\text{-OOCCH}_3)_6(\text{NO})(\text{L})_2]^+$ , where L = 4-acpy (**1**), 4-tbpy (**2**); compounds **3** (4-pic = 4-methylpyridien) and **4** (3-pic = 3-methylpyridine) are from literature papers [16, 17].

## 2. Results and discussion

### 2.1 Chemical characterization

As shown in Figure 1, we prepared clusters **1** and **2** by passing a continuous  $\text{NO}(\text{g})$  flow through a solution of the precursor  $[\text{Ru}_3(\mu_3\text{-O})(\mu\text{-OOCCH}_3)_6(\text{H}_2\text{O})(\text{L})_2]\text{PF}_6$  (where L = 4-acpy or 4-tbpy) in dichloromethane (DCM) at ambient temperature, which afforded a

violet solid after purification [16–20]. Elemental analysis, cyclic voltammetry, and UV-vis, IR,  $^1\text{H}$  NMR, and EPR spectroscopies helped to determine the structure and purity of complexes **1** and **2**. Table 1 lists part of these data (Full data are provided as Supplementary Material, Figures S1–S9).

We assigned the data in Table 1 by comparison with similar complexes [17, 19, 20]. Clusters **1** and **2** display the typical profile of the electronic spectra (Figures S3 and S4) of complexes in which the cluster to ligand charge transfer bands (CLCT) due to charge transfer from the metallic center  $[\text{Ru}_3\text{O}]^+$  to both pyridinic and NO ligands emerge below 600 nm. The intra-cluster (IC) band, which involves transitions centered in states that are predominantly metallic in nature, arises between 700 and 800 nm [17].

The cores of the nitrosyl clusters **1** and **2** bear three ruthenium ions in the oxidation state +3 ( $\text{Ru}^{\text{III}}\text{Ru}^{\text{III}}\text{Ru}^{\text{III}}$ ). Thus, this kind of complex has formal charge +1 ( $[\text{Ru}_3\text{O}]^+$ , oxidized form). Following the electron distribution in their molecular orbital diagram under  $D_{3h}$  symmetry  $((a''_2)^2 (e')^4 (a'_1)^2 (e')^4 (e'')^4 (a'_2)^1)$ , there is an unpaired electron, which responsible for the effect named paramagnetic anisotropy [16–20, 30–33]. In the NMR spectra, this effect disturbs the typical chemical shift values of the different  $^1\text{H}$  nuclei, displacing the values of the coordinated ligands as compared to the free species (chemical shift values for both complexes are available in the experimental section) [2, 16–20, 34–39].

**Table 1:** Absorption (UV-vis) and electrochemical data collected from acetonitrile (ACN) solutions and IR data collected from KBr pellets for clusters **1** and **2**

$\lambda_{\text{max}}$ (nm) / $\log \epsilon$ ( $\text{L mol}^{-1} \text{cm}^{-1}$ )				
Clusters	IC*	CLCT** 1	CLCT 2	CLCT 3
<b>1</b>	756/ 2.87	553/ 3.24	456/ 3.32	354/ 3.74
<b>2</b>	707/ 3.04	544/ 2.73	458/ 3.30	-----
IR data ( $\text{cm}^{-1}$ )				
Clusters	$\nu(\text{NO})$	$\nu_{\text{as}}(\text{COO}^-)$		
<b>1</b>	1874	1584		
<b>2</b>	1870	1591		
Electrochemical data $E_{1/2}$ (V vs. Ag/AgCl)				
Clusters	$[\text{Ru}_3\text{O}]^{-1/0}$	$[\text{Ru}_3\text{O}]^{0/+1}$	$[\text{Ru}_3\text{O}]^{+1/+2}$	
<b>1</b>	-0.70	-0.06	1.34	
<b>2</b>	-0.81	-0.09	1.36	

The absorption spectra of clusters **1** and **2** were recorded in ACN ( $10^{-3}$  M). IC\* = intra-cluster transition. CLCT\*\* = cluster-to-ligand charge transfer transition. The cyclic voltammograms of clusters **1** and **2**

were obtained in ACN solution containing 0.1 M TBAPF<sub>6</sub> (TBA = tetrabutylammonium cation); all the data are reported against the Ag/AgCl reference electrode.

In the particular case of nitrosyl trinuclear complexes, the paramagnetic anisotropy effect is partially removed. This happens because severe orbital mixing occurs between the metallic unit and NO, to culminate in pairing of the unpaired electron of the [Ru<sub>3</sub>O]<sup>+</sup> core and the unpaired electron of the NO<sup>0</sup> ligand [16–20]. As a result, nitrosyl clusters and complexes in the reduced form ([Ru<sub>3</sub>O]<sup>0</sup>) present similar magnetic behavior, since chemical reduction causes electron pairing. The NMR and EPR data collected in this work confirm this fact. The EPR spectra of clusters **1** and **2** do not exhibit any signals, which reinforces strong coupling between the NO<sup>0</sup> π\* electron and the ruthenium metal ion dπ electron (<sup>1</sup>H NMR and EPR spectra of clusters **1** and **2** – Figures S6, S7 and S8, S9 respectively – are shown in Supplementary Material).

## 2.2 NO release from clusters **1** and **2** by photo and/or redox stimuli

Complexes **1** and **2** are poorly soluble, so we conducted photolysis in organic medium. Table 2 summarizes the photoinduced NO release yields; spectral changes observed during irradiation are available as Supplementary Material, Figures S10 and S11. Irradiation of clusters **1** or **2** in the region of their charge transfer transition decreases the bands at 756 and 707 nm, respectively, and intensifies the band around 700 nm, to give a spectral profile typical of the solvated species [Ru<sub>3</sub>(μ<sub>3</sub>-O)(μ-OOCCH<sub>3</sub>)<sub>6</sub>(S)(L)<sub>2</sub>]PF<sub>6</sub> [2].

**Table 2.** Quantum yields (φ) and concentration of NO<sub>(g)</sub> released from clusters **1** and **2** obtained by photolysis and NOA experiments

Clusters	φ <sub>NO</sub> <sup>a</sup> λ <sub>377 nm</sub>	[NO] <sup>b</sup> /[NO] <sup>c</sup> 10 <sup>-12</sup> M	[NO] <sup>d</sup> /[NO] <sup>e</sup> 10 <sup>-12</sup> M
<b>1</b>	0.23 ± 0.1	1.65 / 2.26	1.08 / 4.04
<b>2</b>	0.61 ± 0.1	2.48 / 4.01	2.82 / 12.4

<sup>a</sup>Quantum yields (φ) of NO release during photolysis of clusters **1** and **2**, 1.10<sup>-5</sup> M, in ACN solution, calculated with chemical actinometry. <sup>b/c</sup>Concentration of NO<sub>(g)</sub> released from 20- and 40-μL aliquots of cluster solution (ACN, 1.10<sup>-5</sup> M) in the presence of an aqueous ascorbic acid solution (1.10<sup>-5</sup> M). <sup>d/e</sup>Concentration of NO<sub>(g)</sub> released from 60-μL aliquots of cluster solution in the presence of an aqueous ascorbic acid solution (1.10<sup>-5</sup> M) and under irradiation (UV lamp) for <sup>d</sup>t<sub>1</sub> = 0 and <sup>e</sup>t<sub>2</sub> = 5 s.

Interestingly, cluster **2** has higher quantum yield than cluster **1**. Our group has recently reported the same observation for analogues containing the CO ligand [40] and attributed the higher quantum yield to the presence of 4-tert-butylpyridine, a more basic ancillary ligand with  $\sigma$ -donor characteristics. In the ground state, these clusters have an 18-electron configuration [19], where the  $[\text{Ru}_3\text{O}]^+$  unit contributes with 17 electrons, and  $\text{NO}^0$  contributes with its unpaired electron. Due to orbital mixing, this ground state resembles the reduced  $[\text{Ru}_3\text{O}]^0$  moiety more closely. Irradiation in the charge transfer region promotes full electronic density transfer from the  $[\text{Ru}_3\text{O}]$  unit to the  $\text{NO} \pi^*$  level during the excited state lifetime. This removes the electronic pairing verified in the ground state, to reduce interaction between the species and consequently prompt NO release. The  $[\text{Ru}_3\text{O}]$  center becomes paramagnetic after NO release, as probed by the photoproduct typical spectral profile (Figures S10 and S11) [17, 19, 20]. Therefore, when the complex is in the excited state, the metallic core formal charge is indeed +1, which is more stabilized by interaction with a  $\sigma$ -donor ancillary ligand such as 4-tbpy as compared to a more  $\pi$ -acid ligand like 4-acpy [17]. Upon return to the ground state, the oxidized profile is maintained, to afford a complex bearing a coordinated solvent molecule instead of the NO ligand.

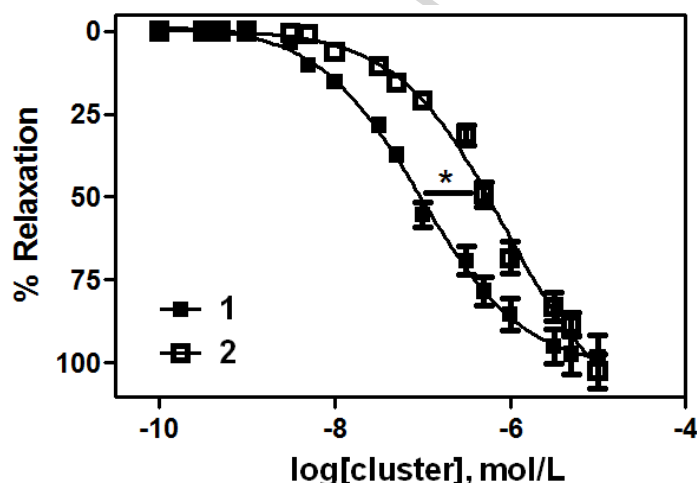
To probe the ability of these complexes to deliver NO under reductive conditions, we determined the concentration of  $\text{NO}_{(\text{g})}$  released from cluster **1** or **2** in the presence of ascorbic acid (Table 2) in the dark and under light irradiation (UV lamp, continuous light). To this end, we employed a NO analyzer (NOA equipment), which detects very low  $\text{NO}_{(\text{g})}$  concentrations under helium flow [41]. The plots of released  $\text{NO}_{(\text{g})}$  detected by NOA are available as Supplementary Material, Figures S12 and S13.

Table 2 revealed that even in small concentrations, NO is delivered because ascorbic acid reduces clusters **1** and **2**. As pointed out above, the main feature that maintains interaction between the  $[\text{Ru}_3\text{O}]^+$  unit and the  $\text{NO}^0$  ligand is pairing of their unpaired electrons in the 18-electron configuration. Reduction of complexes **1** and **2** disrupts this interaction and lowers the affinity of the coordinated NO for the metallic center, ultimately leading to its release. NO release mediated by reduction is also more efficient for complex **2** and, as expected, is boosted by light irradiation (Table 2, third column).

### 2.3 Vasorelaxation caused by cluster **1** or **2** in pre-contracted rat aorta

Knowing that clusters **1** and **2** behave as NO releasers in solution, we investigated two biological properties (vasodilation and cytotoxicity) mediated by NO release. First, we evaluated relaxation by incubating pre-contracted rat aorta without endothelium with cluster **1** or **2**. Figure 2 shows that these clusters induce concentration-dependent relaxation in denuded rat aortas pre-contracted with phenylephrine in the presence of environment light. The maximal effects ( $E_{max}$ ) are  $98.08 \pm 6.40\%$  and  $102.5 \pm 5.10\%$  for clusters **1** and **2**, respectively.

NOA experiments demonstrated that NO release follows reduction of these complexes (with or without light irradiation). In the vasodilation assay, phenylephrine might act as a reducing agent [17]. In fact, we recorded the spectral profile upon reduction of cluster **1** or **2** after reaction with ascorbic acid or phenylephrine, to find that they are essentially the same (Figures S15 and S16). Hence, we attribute the relaxation effect to NO release triggered by the presence of ambient light and phenylephrine.



**Figure 2:** Vasodilator effect of (A)  $[\text{Ru}_3(\mu_3\text{-O})(\mu\text{-OOCCH}_3)_6(\text{NO})(4\text{-acpy})]\text{PF}_6$  (**1**) or (B)  $[\text{Ru}_3(\mu_3\text{-O})(\mu\text{-OOCCH}_3)_6(\text{NO})(4\text{-tbpy})]\text{PF}_6$  (**2**) on rat aorta pre-contracted with phenylephrine ( $0.1 \mu\text{M}$ ) in the presence of environment light. Data are the means  $\pm$  SEM of experiments performed on four preparations obtained from different animals.  $*P < 0.05$ .

Although the vasodilation response is maximum at  $1 \times 10^{-5}$  M, almost 10 times more cluster **2** ( $8 \times 10^{-7}$  M) than cluster **1** ( $1 \times 10^{-7}$  M) is necessary to achieve 50% relaxation. In terms of concentration range, the ability of clusters **1** and **2** to provide 50% and 100% relaxation is quite similar ( $10^{-7}$  to  $10^{-6}$  and  $10^{-5}$  M, respectively) to the behavior reported in the literature for related complexes including **4**,  $[\text{Ru}(\text{NH.NHq})(\text{tpy})\text{NO}]^{3+}$  (tpy = terpyridine),  $\text{trans-}[\text{RuCl}([\text{15}] \text{aneN}_4)\text{NO}]^{2+}$  ([15]aneN4

= 1,5,8,12-tetraazacyclotetraundecane), and the iron complex sodium nitroprusside (SNP) [17, 42–44]. Except for the first example (in which the ancillary ligand is 3-methylpyridine), the other complexes do not bear any structural similarity with the complexes investigated here. Thus, the substituent, or even better, the ancillary ligands themselves, does not influence the vasodilation effect.

#### 2.4 Cytotoxicity studies of nitrosyl clusters **1** and **2**

We examined the *in vitro* cytotoxicity of nitrosyl cluster **1** or **2** against B16F10 (Figure 3) or L929 (Figure 4) cells in the absence or in the presence of light irradiation (at  $\lambda = 527$  nm; dose of 0.25 or 0.41 J/cm<sup>2</sup>). Overall, both clusters are cytotoxic to melanoma cells at different concentration ranges. In addition, relatively low concentrations (25  $\mu$ M) of cluster **2** appear to be toxic to healthy cells. Surprisingly, photostimulation increases the cytotoxicity of complexes **1** and **2** only slightly within the concentrations investigated here. The dark activity of clusters **1** and **2** can be assigned to NO release mediated by reductive processes [16].

At each particular concentration, clusters **1** and **2** are less toxic to non-tumor cells (L929) as compared to the murine melanoma cell line (B16F10) in the dark or upon irradiation with visible light. At 50  $\mu$ M, cluster **1** is not toxic to fibroblast cells at all, but it lowers B16F10 cell viability to 54%. Cluster **2** elicits the same effect on B16F10 cells (approximately 50% of cell viability) at only 1  $\mu$ M. This concentration reduces L929 cell viability to approximately 80%.

Our group was the first to report on the cytotoxicity of a triruthenium cluster; more specifically, complex **3**, toward melanoma cells [16]. In that case, complex **3** at 15  $\mu$ M was necessary to lower B16F10 cell viability to 50%. Light irradiation only raised the cytotoxicity of complex **3** at higher concentration ranges (30 to 60  $\mu$ M). The results of the present work are consistent with the aforementioned behavior and allow us to set the following order of increasing cytotoxicity of triruthenium complexes toward B16F10 melanoma cells with respect to the ancillary ligand: 4-acpy < 4-pic < 4-tbpy.

The cytoplasmic conditions of tumor cells, such as low O<sub>2(g)</sub> concentration, atypical nutrient intake, low pH due to lactic acid production in anaerobic glycolysis, and presence of higher glutathione levels [37,39], often create a favorable environment for reduction processes, which favors NO release from these clusters even in the absence of light irradiation.

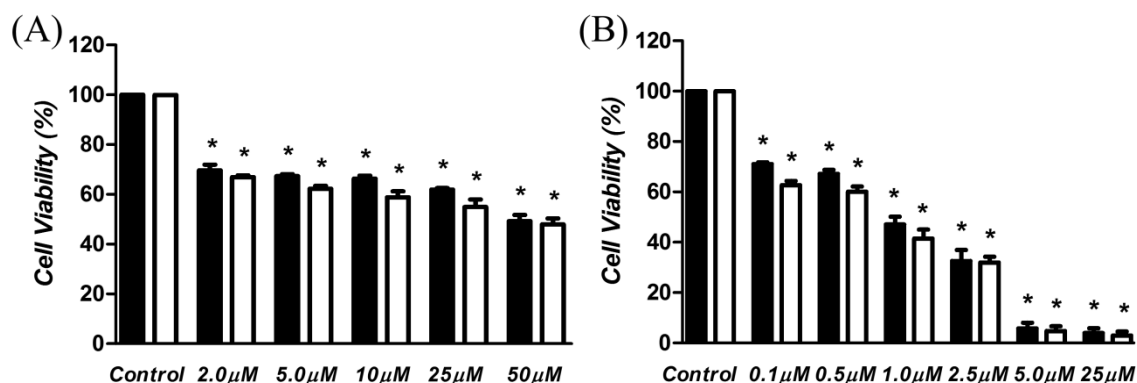


**Figure 3.** Cellular viability of B16F10 cells after treatment with different concentrations of nitrosyl cluster **1** (A) or **2** (B), with (black bars) or without (white bars) light irradiation ( $\lambda=527$  nm; dose of  $0.41$  J/cm<sup>2</sup>) for 24 h. Cell viability was assessed by an MTT assay and expressed as percent of the control. Data are presented as the mean  $\pm$  SEM of three independent experiments. \* is used to represent the statistically significant differences between the treatments and control, considering  $p < 0.05$  according to the ANOVA and post hoc Newman–Keuls tests.

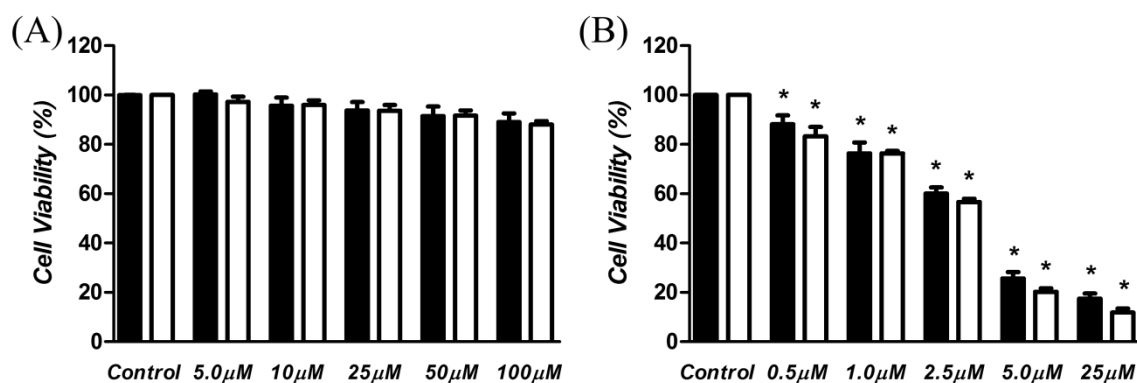


**Figure 4.** Cell viability of L929 cells after treatment with different concentrations of nitrosyl cluster **1** (A) or **2** (B), with (black bars) or without (white bars) light irradiation ( $\lambda=527$  nm; dose of  $0.41$  J/cm<sup>2</sup>) for 24 h. Cell viability was assessed by an MTT assay and expressed as a percent of the control. Data are presented as the mean  $\pm$  SEM of three independent experiments. \* was used to represent the statistically significant differences between the treatments and control, considering  $p < 0.05$  according to the ANOVA and post hoc Newman–Keuls tests.

Presumably, this effect is operating here, to contribute to both the vasorelaxation and cytotoxic activities of complexes **1** and **2**. However, this contribution should be similar for both complexes because the first reduction potentials of clusters **1** and **2** differ only slightly (Table 1), and both are accessible in biological medium. Therefore, the differences in the cytotoxicity of these triruthenium complexes must be a consequence of structural aspects, namely the presence of distinct substituents in the

ancillary pyridinic ligands. More specifically, we realized that higher degree of methylation in the ancillary ligand of complexes **1**, **2**, and **3** [16] results in higher cytotoxicity.

The importance of methylation in modulating biological activity is well documented [45–47]. The methyl group presents many functions and can alter the pharmacological properties of a molecule [24, 45]. Introduction of this group into bioactive compounds makes them more lipophilic/hydrophobic. Hence, the structural differences between clusters **1** (L = 4-acpy) and **2** (L = 4-tbpy) might directly impact processes like internalization, subcellular localization, and interaction with several biomolecules (proteins and/or DNA) or bio-structures including cellular membranes [46].

### 2.5 Interaction of cluster **1** or **2** with Human Serum Albumin (HSA)

To illustrate our point that increased hydrophobicity through methylation promotes interaction with biologically relevant targets, we investigated interaction of cluster **1** or **2** with HSA.

Biological activity is related to association between bioactive compounds and biological targets. This directly affects compound bioavailability, distribution, metabolism, toxicity, and *in vivo* half-life. Therefore, studying the interaction of cluster **1** or **2** with HSA (the major transport protein in blood plasma) is mandatory. We evaluated this interaction by means of HSA fluorescence quenching by cluster **1** or **2**. Here, the assay was considered an indirect method to probe the hydrophobic nature of the complexes under investigation [45–48, 50]. It has recently been shown that compound **4** interacts with HSA through hydrophobic forces; the observed  $K_b$  suggests that HSA can efficiently store and transport this complex in the body [18].

Figures 5A and 5B depict HSA fluorescence quenching in the presence of increasing concentrations of cluster **1** or **2**, respectively. Fluorescence quenching may occur through two distinct mechanisms: static and/or dynamic [51–53]. It is rather difficult to assign which mechanism takes place exclusively on the basis of fluorescence measurements. Usually, it is possible to assign one of the mechanisms by analyzing how  $K_{SV}$  constants vary with temperature. The  $K_{SV}$  quenching constant increases with rising temperature when interaction is dynamic: because this interaction has a collisional nature, it predominates at higher temperature. Nevertheless, static contribution

(formation of a HSA-quencher adduct in the ground state) might be significant even when  $K_{SV}$  increases with temperature. Hence, the quenching mechanism can be determined by comparing the bimolecular quenching constant ( $k_q$ ) and limiting diffusion rate constant of biomolecules ( $kd \approx 2.0 \times 10^{10} \text{M}^{-1} \text{S}^{-1}$ ) [50, 53]. If  $k_q$  is smaller than  $kd$ , dynamic quenching is the main mechanism; otherwise, static quenching prevails [50, 53].

To treat our data, we firstly employed the dynamic Stern-Volmer equation (1).

$$F_0/F = K_{SV}[Q] + 1 = \tau_0 k_q [Q] + 1 \quad (1)$$

where  $F_0$  and  $F$  are the fluorescence intensities in the absence or in the presence of the quencher, respectively;  $K_{SV}$  is the Stern–Volmer quenching constant;  $k_q$  is the bimolecular quenching constant; and  $\tau_0$  is the average lifetime of the excited biomolecule in the absence of a quencher (for HSA,  $\tau_0$  is about  $10^{-8}$  s) [48, 53].

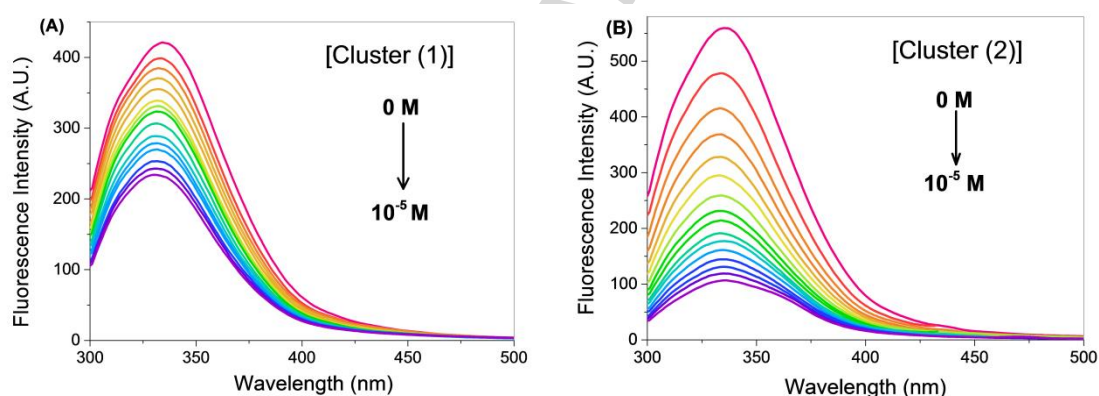


**Figure 5:** Intensity of HSA solution emission with increasing concentration of cluster 1 (A) or cluster 2 (B). ([HSA] = 1.0  $\mu\text{M}$ ) (on the basis of the quencher concentration (0.0 M to  $10^{-5}$  M) during 5-min incubation with HAS).

We obtained the  $K_{SV}$  of systems HSA-1 and HSA-2 at different temperatures from the slopes of  $F_0/F$  versus  $[Q]$  plots (Figure S19) and the  $k_q$  values from the slopes of  $F_0/F$  versus  $[Q] \times \tau_0$  plots (Figure S20). Table 3 presents these values.

$K_{SV}$  increases slightly and significantly with temperature for clusters 1 and 2, respectively. However,  $k_q$  is greater than the diffusion rate constant of the biomolecule ( $k_d$ ) for both complexes, which indicates that static quenching happens between the

clusters and HSA. To confirm this observation, we performed lifetime measurements (Figure S21 and S22). We did not observe variation in the HSA excited state lifetime at any of the investigated temperatures, which attested to static quenching.

**Table 3.** Stern-Volmer quenching constants ( $K_{sv}$  and  $k_q$ ) of the systems HSA-1 and HSA-2 at different temperatures

Cluster	T(K)	$K_{sv}$ ( $M^{-1}$ )	R	$k_q$ ( $M^{-1} S^{-1}$ )	R
<b>1</b>	298	$6.79 \times 10^3$	0.9923	$6.79 \times 10^{11}$	0.9923
	305	$7.06 \times 10^3$	0.9931	$7.06 \times 10^{11}$	0.9931
	312	$8.01 \times 10^3$	0.9951	$8.01 \times 10^{11}$	0.9955
<b>2</b>	298	$9.49 \times 10^7$	0.9986	$9.49 \times 10^{15}$	0.9985
	305	$1.22 \times 10^8$	0.9987	$1.22 \times 10^{16}$	0.9986
	312	$1.12 \times 10^8$	0.9981	$1.12 \times 10^{16}$	0.9981

Furthermore, cluster **2** has atypically high  $K_{sv}$ , even greater than the value obtained for complex **4** and other coordination complexes [18, 55, 56]. Therefore, cluster **2**, which bears the methylated ligand 4-tbpy in its structure, interacts more efficiently with HSA and is a more potent quencher.

Because we concluded that static quenching takes place for the systems HSA-1 and HSA-2, we calculated the binding constant  $K_b$  by using the modified Stern-Volmer equation:

$$\log(F_0-F)/F = \log K_b + n \log[Q] \quad (2)$$

where  $F_0$  and  $F$  are the fluorescence intensities in the absence or in the presence of the quencher, respectively;  $K_b$  is the binding constant; and  $n$  is the average number of interacting clusters (or drug) per protein molecule. Plots of  $\log[(F_0-F)/F]$  versus  $\log[Q]$  yields  $\log K_b$  as the intercept and  $n$  as the slope (Figure S23 and Table S1). For both clusters, the number of interacting clusters per protein unit is close to 1, which suggests that a single binding site is present in the HSA structure in these complexes, and that the stoichiometry is 1:1. On the other hand,  $K_b$  is rather small ( $\sim 10^3 M^{-1}$ ) despite the efficiency with which complexes **1** and **2** quench HSA fluorescence [18, 54].

Together, these results suggests that the nature of the interaction leading to the formation of a ground state adduct between HSA and the clusters must be weak even for complex **2** and presumably does not involve covalent bonds. Alternatively, quenching might occur due to unspecific interactions on the protein surface rather than through binding to specific sites. Indeed, the circular dichroism spectra collected for HSA do not reveal significant changes upon addition of increasing amounts of complexes **1** or **2** (Figure S24), which shows that interaction between these species does not modify HSA conformation upon binding.

The nature of the interaction forces between HSA and a molecule may comprise hydrophobic interactions, hydrogen bonds, van der Waals forces, and electrostatic interactions [18, 54]. Positive enthalpic and entropic changes indicate hydrophobic interactions; negative variations indicate that hydrogen bonds and/or van der Waals forces take place. Finally, negative  $\Delta H$  and positive  $\Delta S$  values attest to electrostatic interaction [52]. We determined the thermodynamic parameters for the interactions between cluster **1** or **2** and HSA according to the following equations:

$$\ln K_b = -\Delta H/RT + \Delta S/R \quad (3)$$

$$\Delta G = -RT \ln K_b \quad (4)$$

where  $K_b$  is the binding constant at a temperature  $T$ , and  $R$  is the gas constant.  $\Delta H$  and  $\Delta S$  are calculated from the slope and intercept values of a  $\ln K_b$  versus  $1/T$  plot, respectively (Figure S25).  $\Delta G$ , which addresses interaction spontaneity, was determined according to equation 4. The obtained values are available in Table S2. Positive  $\Delta H$  and  $\Delta S$  suggest that hydrophobic forces direct binding between cluster **1** or **2** and HSA. For cluster **2**, values are more positive ( $\Delta H = 80.81$  KJ/mol;  $\Delta S = 334.71$  J/Kmol) as compared to complexes **1** ( $\Delta H = 48.10$  KJ/mol;  $\Delta S = 238.02$  J/Kmol) and **4** [18]. This fact highlights the more hydrophobic character of cluster **2** due to the presence of the tert-butyl substituent in the structure of the ancillary ligands. For both clusters studied herein, processes are spontaneous ( $\Delta G > 0$ ).

### 3. Conclusion

We have presented the synthesis and characterization of two novel triruthenium clusters with general formula  $[\text{Ru}_3(\mu_3\text{-O})(\mu\text{-OOCCH}_3)_6(\text{NO})\text{L}_2]\text{PF}_6$ , where  $\text{L} = 4\text{-acetylpyridine}$

(4-acpy, **1**) or 4-tert-butylpyridine (4-tbpy, **2**). Chemical characterization by spectroscopic and electrochemical experiments has demonstrated the proposed structure of the new nitrosyls. In addition, complexes **1** and **2** can release NO in solution under irradiation at  $\lambda_{\text{irrad}} = 377$  nm and through chemical reduction with ascorbic acid.

More interestingly, these compounds have proven to be useful vasodilation agents: they relax pre-contract rat aorta up to 100%. This ability apparently does not depend on the structure of the complexes in our experimental conditions. In contrast, the cytotoxicity of complexes **1** and **2** toward murine melanoma (B16F10 cells) and murine fibroblasts (L929) is related to the structure of the ancillary ligands 4-acpy and 4-tbpy. Cluster **2** has three methyl groups in the ancillary ligands 4-tbpy. This certainly influences the increased cytotoxicity as compared to the results obtained for clusters **1** and **3** [16]. The presence of methyl groups also promotes stronger hydrophobic interactions between cluster **2** and HSA as compared to cluster **1**, which confirms that methylation increases interactions with biomolecules.

All these results allow us to conclude that the choice of ancillary ligands is critical to define the cytotoxic potential of the candidate drug when dealing with the design of metallo drugs. However, the search for compounds with higher cytotoxicity obtained through introduction of hydrophobic CH<sub>3</sub> groups is a controversial issue—methylation also increases cytotoxicity to healthy cells, as demonstrated here for cluster **2** at concentrations above 25  $\mu$ M. At this point, our data do not allow us to discuss whether internalization of the whole complex or of the released NO molecule only underlies the observed cytotoxicity. In other words, it is not yet known whether NO is released outside or inside the cells. Nevertheless, our results constitute an interesting example of how a molecule with increased hydrophobicity (through methylation) enhances its interaction with biotargets and its cytotoxicity.

## 4. Experimental Section

### 4.1 Preparation and Purification

Complexes **1** and **2** were synthesized according to modifications of the procedure published by Toma et al. [18, 19].

$[\text{Ru}_3(\mu_3\text{-O})(\mu\text{-OOCCH}_3)_6(\text{NO})(\text{L})_2]\text{PF}_6$  ( $\text{L} = 4\text{-acpy}$  (**1**) and  $4\text{-tbpy}$  (**2**)). The precursors of  $[\text{Ru}_3(\mu_3\text{-O})(\mu\text{-OOCCH}_3)_6(\text{H}_2\text{O})(4\text{-acpy})_2]\text{PF}_6$  (0.40 g) (**1a**) and  $[\text{Ru}_3(\mu_3\text{-O})(\mu\text{-$

$\text{OOCCH}_3)_6(\text{H}_2\text{O})(4\text{-tbpy})_2]\text{PF}_6$  (0.40 g) (**2b**) were dissolved in DCM, and the solution was degassed with  $\text{Ar}_{(\text{g})}$  for 20 min. The system was saturated with  $\text{NO}_{(\text{g})}$  for 24 h, and the blue solution became violet. After this reaction time, the reaction medium was evaporated to dryness, and the obtained purple solid was washed with petroleum ether and dried under vacuum in desiccators. Further purification of cluster (**2**) was performed by using alumina as stationary phase and a mixture of 10% ACN and 90% DCM as mobile phase. In this system,  $\text{NO}_{(\text{g})}$  was generated by reaction of nitric acid and copper pellets; two solutions were used as trapping system: concentrated  $\text{NaOH}_{(\text{aq})}$  solution (1 M), to remove  $\text{NO}_2^-_{(\text{g})}$  traces, and DCM solution, to saturate the reaction system solvent. **[Ru<sub>3</sub>( $\mu_3$ -O)( $\mu$ -OOCCH<sub>3</sub>)<sub>6</sub>(NO)(4-acpy)<sub>2</sub>PF<sub>6</sub> (1)**. Yield: 0.26 g, 0.24 mmol, 65% (MW = 1090.72 g/mol). Elemental Analysis Calcd for (Ru<sub>3</sub>O<sub>15</sub>C<sub>19</sub>H<sub>25</sub>N<sub>2</sub>PF<sub>6</sub>) C: 28.63% H: 2.96% N: 3.85% Found: C: 28.41% H: 3.01% N: 3.90%. <sup>1</sup>H NMR (ACN-d<sub>3</sub>, 500 MHz):  $\delta$  (ppm) = 4.37 (12 H, s, CH<sub>3</sub> (a)); 3.48 (6 H, s, CH<sub>3</sub> (b)); 8.64 (4 H, d, *J* = 6.5 Hz, H $\alpha$ ); 4.03 (4 H, d, *J* = 6.5 Hz, H $\beta$ ); 2.70 (6 H, d, *J* = 4.0 Hz, H $\gamma$ ). IR (KBr pellets, cm<sup>-1</sup>): 568  $\delta$  (FPF), 690  $\pi$  (Ru<sub>3</sub>O), 838  $\nu_{\text{as}}$ (PF<sub>6</sub>), 1255  $\delta_{\text{s}}$  (CH<sub>3</sub>) 4-acpy, 1415  $\nu_{\text{s}}$  (COO)Ac, 1589  $\nu$ (pyridine ring), 1700 (C=O) 4-acpy, 3442  $\nu$  (OH).

**[Ru<sub>3</sub>( $\mu_3$ -O)( $\mu$ -OOCCH<sub>3</sub>)<sub>6</sub>(NO)(4-tbpy)<sub>2</sub>PF<sub>6</sub> (2)**. Yield: 0.30 g, 0.27 mmol, 75%; (MW = 1118.96 g/mol). Elemental Analysis Calcd for (Ru<sub>3</sub>O<sub>14</sub>C<sub>21</sub>H<sub>31</sub>N<sub>2</sub>PF<sub>6</sub>) C: 32.20% H: 3.96% N: 3.76% Found: C: 33.40% H: 3.99% N: 3.96%. <sup>1</sup>H NMR (ACN-d<sub>3</sub>, 500 MHz):  $\delta$  (ppm) = 3.79 (12 H, s, CH<sub>3</sub> (a)); 3.15 (6 H, s, CH<sub>3</sub> (b)); 8.22 (4 H, d, *J* = 6.6 Hz, H $\alpha$ ); 4.81 (4 H, d, *J* = 6.6 Hz, H $\beta$ ); 1.53 (18 H, s, H $\gamma$ ). IR (KBR pellets, cm<sup>-1</sup>): 548  $\delta$  (FPF), 693  $\pi$  (Ru<sub>3</sub>O), 830  $\nu_{\text{as}}$ (PF<sub>6</sub>), 1430  $\nu_{\text{s}}$  (COO)Ac, 1591  $\nu$ (pyridine ring), 2940  $\nu$  (CH<sub>3</sub>) 4-tbpy, 2971  $\delta_{\text{s}}$  (CH<sub>3</sub>) 4-tbpy, 3432  $\nu$  (OH).

Warning: in the solid state, especially with exposure to light, we observed some degree of decomposition for this compound, with substitution of NO ligands by solvent molecules of crystallization, which is acetonitrile in this case (from the mobile phase of the chromatographic column). This effect accounts for the poor match of the calculated and experimental values of elemental analysis. The experimental values reported above corresponds to a mixture of the original nitrosyl compound and the solvated species in an approximated ratio of 60% nitrosyl : 40% solvated complex. We performed a <sup>1</sup>H NMR measurement in CD<sub>3</sub>OD in order to probe the presence of acetonitrile in our product. The spectrum profile was the same as the one reported in CD<sub>3</sub>CN, with an additional signal at 2.1 ppm ascribed to acetonitrile present in the sample. We also

performed a control IR experiment in which we measured the spectrum of a freshly prepared KBr pellet of compound **2** and measured it again after 2 days of exposure of compound **2** to ambient light and heat. It was verified, by integration of the nNO band area, the loss of 20% of NO.

#### 4.2 Physical measurements

UV–Vis spectra were recorded on a UV Agilent 8453 spectrophotometer (190–1100 nm) equipped with xenon and tungsten lamps and a quartz cuvette with path length of 1.0 cm. IR spectra were acquired on an IR spectrophotometer Shimadzu Prestige 21 (400–4000  $\text{cm}^{-1}$  with resolution 4  $\text{cm}^{-1}$ ), from KBr pellets.  $^1\text{H}$  NMR spectra were obtained on a Bruker Avance DRX- 500 500 MHz from  $10^{-2}$  M  $\text{CD}_3\text{CN}$  solutions. EPR spectra were recorded in a Bruker EMX instrument operating at the X-band (frequency = 9.48 GHz, power = 20mW, modulation frequency = 100 kHz, modulation amplitude = 5–15 G), at 77 K, in the solid state and in ACN solution; Wilmad quartz tubes were used. Cyclic voltammetry experiments were performed in a conventional three-electrode cell (platinum as working electrode, platinum wire as auxiliary electrode, and Ag/AgCl as reference electrode). The supporting electrolyte was tetrabutylammonium hexafluorophosphate ( $\text{TBAPF}_6$ ) 0.1 M. Cluster solutions ( $10^{-3}$  M) were prepared in ACN. Lifetime measurements were recorded on Tsunami - Spectra Physics; the selected excitation wavelength was 281 nm at three incubation temperatures (298, 305, or 310 K). To a HSA solution ( $1.0 \times 10^{-6}$  M), successive aliquots of cluster **1** or cluster **2** solutions (0,  $1.4 \times 10^{-5}$ ,  $1.8 \times 10^{-5}$ ,  $2.2 \times 10^{-5}$ ,  $2.6 \times 10^{-5}$ , or  $3.0 \times 10^{-5}$  M), both prepared in Trizma<sup>®</sup> buffer, were added. The signal detected as pulse excitation is called IRF (instrument response function). The resulting curves were fitted by an exponential adjust of the program Origin 8.0<sup>®</sup>. Circular Dichroism spectra were registered with a Jasco 810 Spectropolarimeter (Jasco, Hachioji City, Tokyo, Japan). HSA ( $1.0 \times 10^{-6}$  M) CD spectra in the presence of complex **1** or **2** were acquired in a 1-cm quartz cuvette in Trizma<sup>®</sup> buffer solutions (complex concentration:  $1.5 \times 10^{-5}$ ,  $2.5 \times 10^{-5}$ , or  $3.0 \times 10^{-5}$  M).

#### 4.3 NO release experiments

NO release from clusters **1** or **2** was evaluated by two methods. Photolysis of cluster **1** or **2** was accomplished from  $10^{-5}$  M solutions in ACN in quartz cuvette with optical path of 1 cm. Solutions were stirred continuously during the irradiation time (2 min,  $\lambda = 377$

nm). Irradiation was performed with a diode laser Colibri QuantumTech®. Light intensities were determined by chemical actinometry (ferrioxalate salts) in order to calculate quantum yields. The second method was based on a General Electric model NOA-280i nitric oxide analyzer (NOA) under helium flow, which helped to analyze the generated NO. NO was detected in the absence of ambient light; an ascorbic acid aqueous solution ( $10^{-5}$  M) was used as reducing agent. First, 20 or 40  $\mu\text{L}$  of cluster **1** or **2** in ACN solution ( $10^{-5}$  M) was added to the system. NO was detected in the presence of UV irradiation. To this end, 60  $\mu\text{L}$  of cluster **1** or **2** in ACN ( $10^{-5}$  M) was added to the system, followed by irradiation with a UV lamp for 5 s (The Graphs are in SI-1 and SI-2). The number of NO moles was based on the straight line obtained from the analytical curve (Supplementary Data) of the device; the full area was based on the release curve.

#### *4.4 Vasodilation assay and aortic ring preparation*

Experiments were conducted in accordance with the Animal Ethics Committee, Ribeirão Preto Campus, University of São Paulo, Brazil, under environment light. The vasodilation assay was conducted in a bath system for isolated organs; the vascular reactivity procedure was employed. First, Male Wistar rats (180-200 g) were stunned by inhalation of isoflurane, euthanized by decapitation, and exsanguinated. The descending thoracic aorta was rapidly dissected and cut into rings (4-mm length). Endothelium was mechanically removed by gently rubbing the vessel surface of the rings with a thin wire. Rings were maintained in a 10-mL organ chamber containing Krebs buffer solution with the following composition (mM): NaCl 130, KCl 4.7,  $\text{KH}_2\text{PO}_4$  1.2,  $\text{MgSO}_4$  1.2,  $\text{NaHCO}_3$  14.9, glucose 5.5, and  $\text{CaCl}_2$  1.6. The solution was maintained at pH 7.4 and gassed with 95%  $\text{O}_2$  and 5%  $\text{CO}_2$  at 37 °C. Initially, rings were stretched to a basal tension of 1.5 g (previously determined by length–tension relationship experiments), before they were allowed to equilibrate for 60 min in the bath fluid, which was changed every 15–20 min. Since our studies required endothelium-denuded aorta, endothelial integrity was qualitatively assessed by the degree of relaxation caused by acetylcholine (ACh, 1 M) in the presence of a contractile tone induced by phenylephrine (0.1  $\mu\text{M}$ ). Absence of endothelium was confirmed by lack of relaxation response to acetylcholine 1  $\mu\text{M}$  in aortic rings pre-contracted with phenylephrine 0.1  $\mu\text{M}$ .

Complex solutions were prepared in water (0.1 nM to 10  $\mu\text{M}$ ) by diluting the stock concentration that had been prepared in DMSO (0.1 mM). To examine how the

complexes affected smooth muscle cell relaxation, aortic rings were pre-contracted with phenylephrine 0.1  $\mu\text{M}$ . When the contraction had reached a plateau, complex solution (0.1 nM to 10  $\mu\text{M}$ ) was cumulatively added.

#### 4.5 Cell Culture

B16F10 (melanome murine) and L929 (fibroblast murine) cells were obtained from the cell bank from the city of Rio de Janeiro. Cells were cultured in 75-cm<sup>2</sup> flasks containing RPMI medium (Roswell Parking Memorial Institute Medium – Gibco®) with 10% defined supplement fetal bovine serum plus penicillin G 100 IU/mL, streptomycin 100 mg/mL, and amphotericin 1  $\mu\text{g}/\text{mL}$ . Cells were cultured until 75–90% confluence in a humidified incubator at 37.0 °C with 5.0% CO<sub>2(g)</sub> for 24 h.

#### 4.6 Cell viability assay

Cytotoxicity of the nitrosyl clusters was evaluated against two cell lines, murine melanoma, B16F10, and murine fibroblast, L929. To this end,  $2 \times 10^4$  cells were incubated in 96-well cell culture plates for 24 h. After this period, treatment with cluster 1 (2.0, 5.0, 10, 25, 50, or 100  $\mu\text{M}$ ) or cluster 2 (0.1, 0.5, 1.0, 2.5, 5.0, or 25  $\mu\text{M}$ ) previously dissolved in DMSO was conducted with or without light irradiation ( $\lambda = 527$  nm; dose of 0.25 or 0.41 J/cm<sup>2</sup>). Graphs obtained at 0.25 J/cm<sup>2</sup> are available as Supplementary Data (S15). After the incubation time, cell viability was evaluated by the MTT (3-(4,5-dimethylthiazol-2-yl)-2,5-ditetrazolium bromide) colorimetric assay; wells that did not contain any of the complexes were used as control [29]. The blue MTT formazan precipitate was then dissolved in 100  $\mu\text{L}$  of DMSO, and absorbance at 492 nm was measured on a VARIAN CARY-50MPR multi-well plate reader. Cell viability is expressed as the percentage of these values in treated cells as compared to non-treated (control) cells. All experiments were carried out in triplicates on different occasions. Data are presented as the mean  $\pm$  standard error of triplicate cultures. For statistical significance, differences were considered at the 0.05 level of significance with  $p \leq 0.05$ ; One-way ANOVA- Newman-Keuls Multiple Comparison Test was used to compare results from different treatments. Complexes were dissolved in DMSO and then in the culture medium and serially diluted to the appropriate concentration, to give a final DMSO concentration of 1%.

#### 4.7 Complex interaction with HSA

The interaction of the complexes with human serum albumin (HSA) was assayed in the absence of ambient light, to ensure that the investigated species were the nitrosyls. HSA was purchased from Sigma-Aldrich. Stock HSA solutions were prepared in aqueous tris-buffer (pH = 7.2,  $10^{-4}$  M) solutions on the basis of its molecular weight (66,463Da) and kept refrigerated at 10 °C. A stock solution ( $10^{-3}$  M) of cluster **1** or **2** was prepared in ACN ( $0$  M –  $1 \times 10^{-5}$  M). Measurements were carried out at three incubation temperatures (298, 305, or 312 K). Initially, the spectrum of the solution containing HAS only was recorded after incubation for 5 min to adapt the conformation of the macromolecule to the monitoring temperature. Sequentially, aliquots (30 uL) of on of the complexes were added, and 2-min incubation was allowed before the luminescence spectrum was recorded.

#### 4.8 Fluorescence measurements

HSS fluorescence spectra at different temperatures were recorded on a Shimadzu fluorescence spectrophotometer, model RF-5301PC, in a quartz cell with optical path of 1.0 cm. The fluorescence spectrophotometer was set up with excitation and emission slit widths of 5 nm. The wavelength 280 nm was used for sample excitation. The fluorescence intensities were corrected for absorption of the exciting light and inner filter effects by means of the equation:

$$F_{corr} = F_{obs} e^{(A_{exc}+A_{em})/2}$$

where  $F_{cor}$  and  $F_{obs}$  represent the corrected and observed fluorescence intensities, and  $A_{ex}$  and  $A_{em}$  are the absorbance of protein and ligand at the excitation and emission wavelengths, respectively.

#### Acknowledgements

This work was supported by the Brazilian agencies Fundação de Amparo a Pesquisa do Estado de São Paulo (FAPESP, grant number 2015/20302-7 and 2014/25561-8) and Conselho Nacional de Desenvolvimento Científico e Tecnológico (CNPq, grant number 305415/2015-8). We thank Dra. Ana Maria da Costa Ferreira (IQ, USP) for the EPR analysis; Prof. Lusiane Bendhack and PhD Michele Paulo (FCFRP, USP) for the

vasorelaxation experiments; Prof. Amando S. Ito (FFCLRP, USP) for the use of the Tsunami - Spectra Physics spectrophotometer; and Dr. Juliana Cristina Moraes Biazzotto, Clovis Junior, and Prof. Dr. Roberto Santana da Silva (FCFRP, USP) for their help with the acquisition of *in vitro* anti-cancer data.

#### Abbreviation List

4-acpy = 4-acetylpyridine

4-tbpy = 4-tert-butylpyridine

4-pic = 4-methylpyridine

3-pic = 3-methylpyridine

ACN = acetonitrile

CLCT = cluster-to-ligand charge transfer

DCM = dichloromethane

DMSO = dimethylsulfoxide

IC = intra-cluster transition

HSA = human serum albumin

MTT = 3-(4,5-dimethylthiazol-2-yl)-2,5-diphenyltetrazolium bromide

NOA = NO analyzer

TBA = tetrabutylammonium

#### Appendix A. Supplementary data

Supplementary data related to this article can be found at [http:// dx.doi.org](http://dx.doi.org)

#### References

- [1] A.W. Mond, The acetates of ruthenium, *J. Am. Chem. Soc.* (Resumed) (1930) 1247-1249.
- [2] H.E. Toma, K. Araki, A.D.P Alexiou, S. Nikolaou, S. Dovidauskas. Monomeric and extended oxo-centered triruthenium clusters. *Coord. Chem. Rev.* 221 (2001) 187–234.
- [3] G.D. Starla, J.C. Goeltz, B.J. Lear, C.P. Kubiak. Inter-or intramolecular electron transfer between triruthenium clusters: we'll cross that bridge when we come to it. *Coord. Chem. Rev* 254 (2010) 331-345.
- [4] G.C. John, E.E. Benson, C.P. Kubiak. Electronic structural effects in self-exchange reactions. *J. Phys. Chem. B.* 114 (2010) 14729-14734.

- [5] A.D.P. Alexiou, H.E. Toma. NMR Spectroscopic Correlations for a Series of Triangular  $\mu$ -Oxoruthenium Acetate Clusters containing Substituted Pyridine Ligands. *J. Chem. Research (S)*. 9 (1997) 338-339.
- [6] S.H. Toma, J.J. Santos, K. Araki, H.E. Toma. Supramolecular Approach to Gold Nanoparticle/Triruthenium Cluster Hybrid Materials and Interfaces. *Eur. J. Inorg. Chem.* 10 (2011) 1640-1648.
- [7] S. Nikolaou, A.L.B. Formiga, H.E. Toma. Probing the electronic delocalization in a cyclic pyrazine ruthenium cluster hexamer. *Inorg. Chem. Commun.* 9 (2010) 1032-1035.
- [8] S. H. Toma, J. J. Santos, S. Nikolaou, K. Araki, H. E. Toma. Direct assembly of a metallodendrimer encompassing seven triruthenium clusters units. *Inorganica Chim. Acta.* 390 (2012) 148-153.
- [9] H. Zhang, Y. Sasaki, M. Abe, Y. Zhang, S. YE, M. Osawa, K. Uosaki. Electrochemical and infrared spectroscopic study of the self-assembled monolayer of a cyano-bridged dimeric triruthenium complex on gold surface. *J. Electroanal. Chem.* (2014) 51-55.
- [10] Z. Hua-Xin, Y. Sasaki, Y Zhang, S. Ye, M.O. Masaaki Abe, K. Uosaki. Synthesis and properties of the cyano complex of oxo-centered triruthenium core  $[\text{Ru}_3(\mu_3\text{-O})(\mu\text{-CH}_3\text{COO})_6(\text{pyridine})_2(\text{CN})]$ . *Inorg. Chem.* 3 (2013)1288-1294.
- [11] S. Nikolaou, H.E. Toma. A Convergent Approach for the Generation of Dendrimers Containing the  $[\text{Ru}_3\text{O}(\text{CH}_3\text{COO})_6]$  Electroactive Core. *Eur. J. Inorg. Chem* 14 (2008) 2266-2271.
- [12] L. Mimi, Z. J. Lim, Y. Y. Gwee, A. Levina, P. A. Lay. Characterization of a Ruthenium (III)/NAMI-A Adduct with Bovine Serum Albumin that Exhibits a High Anti-Metastatic Activity. *Angew. Chem. Int. Ed.* 9 (2010) 1661-1664.
- [13] T. Jiří, L.E.H Paul, J. Furrer, B. Therrien, G. Süß-Fink. Cationic triruthenium (III) oxo complexes of the type  $[\text{Ru}_3\text{O}(\text{OAc})_6\text{L}_3]^+$  containing imidazole, pyrazole, thiazole and oxazole ligands: Synthesis, molecular structure, and cytotoxicity. *Inorganica Chim. Acta* 423 (2014) 16-20.
- [14] O. Hiroyoshi, N. Fujiwara, T. Yamaguchi. Mixed-Valence State of a Pyrazine-Bridged Dimer of Oxocarboxylatotriruthenium Complexes with a Nitrosyl Ligand. *Inorg. Chem.* 16 (2011) 7382-7384.
- [15] L. Benjamin, C. P. Kubiak. Charge gating and electronic delocalization over a dendrimeric assembly of trinuclear ruthenium clusters. *Inorg. Chem* 18 (2006) 7041-7043.

- [16] Z.A. Carneiro, J.C. Biazzotto, A.D. P Alexiou, S. Nikolaou. Nitric oxide photorelease from a trinuclear ruthenium nitrosyl complex and its in vitro cytotoxicity against melanoma cells. *J. Inorg. Biochem.* 134 (2014) 36-38.
- [17] N. Cacita, B. Possato, C.F.N. Silva, M. Paulo, A. L. B. Formiga, L. M. Bendhack, S. Nikolaou. Investigation of a novel trinuclear  $\mu$ -oxo ruthenium complex as a potential nitric oxide releaser for biological purposes. *Inorg. Chim. Acta.* 429 (2015) 114-121.
- [18] N. Cacita, S. Nikolaou. Studying the interaction between trinuclear ruthenium complexes and human serum albumin by means of fluorescence quenching. *J. Lumin.* 169 (2016) 115-120.
- [19] H.E. Toma, A.D.P Alexiou, S. Dovidauskas. Extended Electronic Interactions in a Triangular  $\mu$ -Oxotruthenium Acetate Cluster Containing Nitric Oxide. *Eur. J. Inorg. Chem* 11 (2002) 3010-3017.
- [20] H. E. Toma, A.D.P Alexiou, A.L.B. Formiga, M. Nakamura, S. Dovidauskas, M. N. Eberlin, D. M. Tomazela. A nitric oxide releaser based on the  $\mu$ -oxo-hexaacetate-bis (4-methylpyridine) triruthenium nitrosyl complex. *Inorganica Chim. Acta* 358 (2005) 2891-2899.
- [21] Z. Wei, Y. Zhang, M. Abe, K. Uosaki, M. Osawa, Y. Sasaki, S. Ye. Surface coordination of nitric oxide to a self-assembled monolayer of a triruthenium cluster: An in situ infrared spectroscopic study. *Langmuir* 15 (2008) 8027-8035.
- [22] Z. Yi, Y. Tong, M. Abe, K. Uosaki, M. Osawa, Y. Sasaki, S. Ye. Fabrication of photochemical pattern on a self-assembled monolayer (SAM) of a ruthenium cluster under electrochemical control. *J. Mater. Chem.* 2 (2009) 261-267.
- [23] S. Yoichi, M. Abe. Ligand–ligand redox interaction through some metal-cluster units. *Chem. Rec.* 5 (2004) 279-290.
- [24] E J. Barreiro, A. E. Kümmerle, C.A.M. Fraga. The methylation effect in medicinal chemistry. *Chem. Rev.* 9 (2011) 5215-5246.
- [25] D. Bonaventura, R.G. Lima, J. A. Vercesi, R. S. Silva, L. M. Bendhack. Comparison of the mechanisms underlying the relaxation induced by two nitric oxide donors: sodium nitroprusside and a new ruthenium complex. *Vasc. Pharmacol.* 3 (2007) 215-222.
- [26] E.J. Barreiro, C.A.M. Fraga. *Química Medicinal-: As bases moleculares da ação dos fármacos.* Artmed Editora, 2014.
- [27] K.C. Chu, In *The Basis of Medicinal Chemistry/Burger's Medicinal Chemistry*; John Wiley: New York, 1980.
- [28] P. Bazzini, C. G. Wermuth, In *The Practice of Medicinal Chemistry*; Academic Press: San Diego, 2008.

- [29] T. Mosmann. Rapid colorimetric assay for cellular growth and survival: application to proliferation and cytotoxicity assays. *J. Immunol. Methods.* 65 (1983) 55-63.
- [30] J.A. Baumann, D.J. Salmon, T. Stephen, T. J. Meyer, W. E. H. Field. Electronic structure and redox properties of the clusters  $[\text{Ru}_3\text{O}(\text{CH}_3\text{CO}_2)_6\text{L}_3]^{n+}$ . *Inorg. Chem.* 12 (1978) 3342-3350.
- [31] A. F. Cotton, J. G. Norman. Structural characterization of a basic trinuclear ruthenium acetate. *Inorganica Chim. Acta.* 6 (1972) 411-419.
- [32] H. E. Toma, F. M. Matsumoto, C. Cipriano. Spectroelectrochemistry of the hexanuclear cluster  $[\text{Ru}_3\text{O}(\text{acetate})_6-\mu\text{-(pyrazine)}_3-\{\text{Fe}(\text{CN})_5\}_3]^{n-}$  and of its modified nickel electrode in aqueous solution. *J. Electroanal. Chem.* 2 (1993) 261-270.
- [33] A. Masaaki, Y. Sasaki, A. Nagasawa, T. Ito. Kinetic Studies on the Terminal Pyridine Exchange Reactions of Some Oxo-Acetate Bridged Trinuclear Ruthenium Complexes. Influence of the Metal Oxidation State and Non-Leaving Terminal Ligand (CO). *Bull. Chem. Soc. Jpn.* 5 (1992) 1411-1414.
- [34] K. Nakamoto, *Infrared and Raman Spectra of Inorganic and Coordination Compounds.* 5th ed. John Wiley & Sons INC, 1997.
- [35] D. Teng-Yuan, H. Lee, T. Lee, C. Hsieh. Magnetic and Spectral Properties of Heterotrinnuclear Acetates  $[\text{Ru}_2\text{Co}(\mu_3\text{-O})(\mu\text{-CH}_3\text{CO}_2)_6(\text{Py})_3]^{n+}$  (n= 0 or 1). *Journal of the Chinese Chemical Society.* 5 (1992) 393-399.
- [36] O. Akihiro, A. Tokiwa-Yamamoto, M. Abe, T. Ito, Y. Sasaki, K. Umakoshi, R. D. Cannon. Structure and Vibrational Spectra of Trinuclear Metal Cluster Complexes. A Question of Symmetry. *Chem. Lett.* 2 (1995) 97-98.
- [37] S. Dovidauskas, H. E. Toma, K. Araki, H. C. Sacco, Y. Iamamoto. (5, 10, 15, 20-Tetra (4-pyridil) porphinato) manganese (III) acetate modified by four  $\mu_3$ -oxo-triruthenium acetate clusters: synthesis, characterization, electrochemical behavior and catalytic activity. *Inorganica Chim. Acta.* 2 (2000) 206-213.
- [38] K, Araki, S. Dovidauskas, H. Winnischofer, A.D.P, Alexiou, H. E. Toma. A new highly efficient tetra-electronic catalyst based on a cobalt porphyrin bound to four  $\mu_3$ -oxo-ruthenium acetate clusters. *J. Electroanal. Chem.* 1 (2001) 152-160.
- [39] H.E. Toma, A.DP Alexiou, S. Nikolaou, S. Dovidauskas.  $^{13}\text{C}$  NMR spectra of triangular -oxoruthenium acetate clusters revisited: HETCOR study of two pyridine and 4, 4'-bipyridine derivatives. *Magn. Reson. Chem.* 37 (1999) 322-324.
- [40] M. Moreira, C.F.N. Silva, R.B. Pesci, V. M. Deflon, S. Nikolaou. "Revisiting oxo-centered carbonyl-triruthenium clusters: investigating CO photorelease and some spectroscopic and electrochemical correlations. *Dalton Trans.* 42 (2016) 16799-16809.

- [41] Sievers Nitric Oxide Analyzer Overview. <http://www.geinstruments.com/products-and-services/nitric-oxide-analyzer/>. (accessed 14 August 2016).
- [42] R. G. De lima, M. G. Sauaia, D. Bonaventura, A. C. Tedesco, L. M. Bendhack, R. S. Silva. Influence of ancillary ligand L in the nitric oxide photorelease by the Ru(L)(tpy) NO]<sup>3+</sup> complex and its vasodilator activity based on visible light irradiation. *Inorganica Chim. Acta.* 8 (2006) 2543-2549.
- [43] M. S. P. Marchesi, S. A. Cicillini, A. C. L. Prazias, L. M. Bendhack, A. A. Batista, R. S. Silva. "Chemical mechanism of controlled nitric oxide release from trans-[RuCl([15]aneN<sub>4</sub>)NO](PF<sub>6</sub>)<sub>2</sub> as a vasorelaxant agent. *Transition Met. Chem.* 5 (2012) 475-479.
- [44] R. G. De Lima, B. R. Silva, R. S. Silva, L. M. Bendhack. Ruthenium complexes as NO donors for vascular relaxation induction. *Molecules* 7 (2014) 9628-9654.
- [45] A. E Sales, L. Breydo, T.S. Porto, A.L.F, Porto, V.N Uversky. Hydrophobicity-dependent effects of polymers on different protein conformations. *RSC Advances* 49 (2016) 42971-42983.
- [46] C. S. Leung., S. F. Siegfried, J. Tirado-rives, W. L. Jorgensen. Methyl Effects on Protein–Ligand Binding. *J. Med. Chem.* 55 (2012) 4489–4500.
- [47] N. Bijari, Y. Shokoohinia, M.R. Ashrafi-Shk, S. S. Ranjbar, M. Parvaneh, M. Moieni-Arya, R. Khodarahmi. Spectroscopic study of interaction between osthole and human serum albumin: Identification of possible binding site of the compound. *J. Lumin.* 143 (2013) 328-336.
- [48] J.R. Lakowicz, *Principles of Fluorescence Spectroscopy*, 3rd ed, Kluwer Academic Publisher, New York, Boston, Dordrecht, London, Moscow, 2006.
- [49] E. Alessio. Thirty Years of the Drug Candidate NAMI-A and the Myths in the Field of Ruthenium Anticancer Compounds: A Personal Perspective. *Eur. J. Inorg. Chem.* 12 (2017) 1549 - 1560.
- [50] W.R Ware. Oxygen quenching of fluorescence in solution: an experimental study of the diffusion process. *J. Phys. Chem.* 3 (1962) 455-458.
- [51] J. Min, X. Meng-xia, Z. Dong, L. Yuan, L. Xiao-yu, C. Xing. Spectroscopic studies on the interaction of cinnamic acid and its hydroxyl derivatives with human serum albumin. *J. Mol. Struct.* 1 (2004) 71-80.
- [52] R. Liu, X. Yu, W. Gao, D. Ji, F. Yang, X. Li, J. Chen, H. Tao, H. Huang, P. Yi. Study on the interaction between salvianic acid A sodium and bovine serum albumin by spectroscopic methods. *Spectrochimica Acta Part A: Molecular and Biomolecular Spectroscopy.* 5 (2011) 1535-1539.

[53] T.G. Dewey. *Biophysical and Biochemical Aspects of Fluorescence Spectroscopy*, first ed., Springer, US, New York, 1991.

[54] N. Bijari, Y. Schokoohinia, M.R. Ashrafi-kooshk, S. Ranjbar, S. Parvaneh, M. Moieni-arya, R. Khodarahmi. Spectroscopic study of interaction between osthole and human serum albumin: Identification of possible binding site of the compound. *J. Lumin.* 143 (2013) 328-336.

[55] P.D. Ross, S Subramanian. Thermodynamics of protein association reactions: forces to stability. *Biochemistry* 20 (1981) 3096 - 3102.

[56] J.T Peters. *All About Albumin: Biochemistry, Genetics, and Medical Applications*, Academic Press: San Diego, 1996.

ACCEPTED MANUSCRIPT